European Radiology (2019) 29:3017–3026
https://doi.org/10.1007/s00330-018-5811-6

CARDIAC

Fractional flow reserve derived from CCTA may have a prognostic role in myocardial bridging

Fan Zhou[1] · Chun Xiang Tang[1] · U. Joseph Schoepf[1,2] · Christian Tesche[2,3] · Maximilian J. Bauer[2] · Brian E. Jacobs[2] · Chang Sheng Zhou[1] · Jing Yan[4] · Meng Jie Lu[1] · Guang Ming Lu[1] · Long Jiang Zhang[1]

Received: 12 May 2018 / Revised: 12 September 2018 / Accepted: 27 September 2018 / Published online: 30 October 2018

Abstract

Purpose To evaluate the feasibility of fractional flow reserve (cFFR) derivation from coronary CT angiography (CCTA) in patients with myocardial bridging (MB), its relationship with MB anatomical features, and clinical relevance.

Methods This retrospective study included 120 patients with MB of the left anterior descending artery (LAD) and 41 controls. MB location, length, depth, muscle index, instance, and stenosis rate were measured. cFFR values were compared between superficial MB (≤ 2 mm), deep MB (> 2 mm), and control groups. Factors associated with abnormal cFFR values (≤ 0.80) were analyzed.

Results MB patients demonstrated lower cFFR values in MB and distal segments than controls (all $p < 0.05$). A significant cFFR difference was only found in the MB segment during systole between superficial (0.94, 0.90–0.96) and deep MB (0.91, 0.83–0.95) ($p = 0.018$). Abnormal cFFR values were found in 69 (57.5%) MB patients (29 [49.2%] superficial vs. 40 [65.6%] deep; $p = 0.069$). MB length (OR = 1.06, 95% CI 1.03–1.10; $p = 0.001$) and systolic stenosis (OR = 1.04, 95% CI 1.01–1.07; $p = 0.021$) were the main predictors for abnormal cFFR, with an area under the curve of 0.774 (95% CI 0.689–0.858; $p < 0.001$). MB patients with abnormal cFFR reported more typical angina (18.8% vs 3.9%, $p = 0.023$) than patients with normal values.

Conclusion MB patients showed lower cFFR values than controls. Abnormal cFFR values have a positive association with symptoms of typical angina. MB length and systolic stenosis demonstrate moderate predictive value for an abnormal cFFR value.

Key Points

- *MB patients showed lower cFFR values than controls.*
- *Abnormal cFFR values have a positive association with typical angina symptoms.*
- *MB length and systolic stenosis demonstrate moderate predictive value for an abnormal cFFR value.*

Keywords Computed tomography angiography · Fractional flow reserve · Myocardial bridging

Abbreviation

AUC	Area under the curve
CAD	Coronary artery disease
CCTA	Coronary computed tomography angiography
CFD	Computational fluid dynamics
cFFR	CCTA-derived fractional flow reserve
DML	Deep-machine-learning
LAD	Left anterior descending coronary artery
MB	Myocardial bridging
OR	Odds ratio
ROC	Receiver operating characteristic

✉ Long Jiang Zhang
kevinzhlj@163.com

[1] Department of Medical Imaging, Jinling Hospital, Medical School of Nanjing University, Nanjing 210002, Jiangsu, China

[2] Division of Cardiovascular Imaging, Department of Radiology and Radiological Science, Medical University of South Carolina, Ashley River Tower, MSC 226, 25 Courtenay Dr, Charleston, SC 29425, USA

[3] Department of Cardiology and Intensive Care Medicine, Heart Center Munich-Bogenhausen, Munich, Germany

[4] Siemens Healthcare Ltd., No. 278 ZhouZhu Road, Shanghai 201318, China

Introduction

Myocardial bridging (MB) is a common congenital coronary artery variant that most commonly affects the mid-portion of the left anterior descending coronary artery (LAD) [1, 2]. MB is ordinarily considered a benign incidental finding [3–6]; however, a small subset of patients without obstructive coronary artery disease (CAD) develop clinical complications

including ischemia, acute coronary syndrome, and sudden death [2, 7–9]. Symptoms may develop or progress as the patient ages [8]. In addition, atherosclerotic plaque can accumulate in regions proximal to the MB, possibly due to dynamic retrograde flow in the LAD from compression of the bridged vessel segment [9, 10]. Evaluating the hemodynamic significance of MB may therefore be clinically relevant with the potential to benefit a subset of MB patients.

MB is frequently found on coronary computed tomography angiography (CCTA). Typical findings associated with MB on CCTA include intramyocardial course of a coronary artery segment as well as the presence of the milking effect phenomenon [11–13]; however, CCTA is a priori that is unable to accurately assess the hemodynamic relevance of MB. Thus, risk stratification of MB patients remains difficult using findings from conventional CCTA, and physiologic assessment is considered superior to the anatomical assessment for evaluating the clinical relevance of MB [14].

A recent study showed intracoronary physiology evaluation with fractional flow reserve (FFR) or instantaneous wave–free ratio (iFR) to be much more effective than a strictly anatomical evaluation in unmasking the hemodynamic significance of MBs [15]. CCTA-derived fractional flow reserve (cFFR) has been used for the noninvasive assessment of lesion-specific ischemia and has shown high diagnostic performance in patients with stable CAD [16]. However, to date, the role of cFFR in the evaluation of patients with MB has not been investigated [8].

Therefore, the purpose of this study was to evaluate the feasibility of cFFR use in patients with MB, its relationship with MB anatomical features, and its clinical relevance.

Methods

Subjects

This retrospective study was approved by the local institutional review board with a waiver for written informed consent. A search of the Picture Archiving and Communication System at our institution generated 4914 patients who underwent CCTA between May 1, 2016, and April 30, 2017. For MB patients, only MBs located in the LAD were studied. Exclusion criteria included any concomitant atherosclerotic disease regardless of the degree of coronary artery stenosis, left ventricular hypertrophy and valvular disease, previous percutaneous coronary intervention or coronary artery bypass grafting, implanted cardiac devices, and anomalous coronary arteries as evidenced by conventional CCTA. Patients with a CCTA image quality score of 1 that were deemed unsuitable for cFFR analysis in either cardiac phase and patients who underwent CCTA with different CT scanners or acquisition modes were excluded from the study. In addition, 41 age- and sex-matched subjects with negative CCTA findings meeting the same enrollment criteria were randomly selected as a control group. The final study population included 120 patients with LAD MB and 41 control subjects. The study flowchart is represented in Fig. 1.

Patient medical history was reviewed and chest pain was classified and recorded as either typical, atypical, nonanginal, or absent [17]. Typical chest pain was defined as follows: (a) substernal chest discomfort with a characteristic quality and duration that is (b) provoked by exertion or emotional stress and (c) relieved by rest or nitroglycerin. Atypical angina was considered chest discomfort that lacks one of the aforementioned characteristics. Nonanginal chest pain was defined as chest discomfort that met one or none of the typical angina characteristics. In patients without chest pain, other symptoms such as syncope, dyspnea, and palpitations were recorded [17].

CCTA protocols

Scanning protocols

All subjects received sublingual nitroglycerin (0.1 mg per dose, Nitroglycerin Inhaler) 5 min prior to CCTA acquisition. Beta-blockers were not administered to any of the patients. CT examinations were performed on a second-generation dual-source CT system (Somatom Flash; Siemens Healthineers). All 161 patients underwent CCTA using prospectively ECG-triggered adaptive sequence acquisition. Acquisition parameters were as follows: detector collimation, 64 × 2 × 0.6 mm; gantry rotation time, 280 ms; and effective tube current–time product, 370 mAs per rotation. For all studies, automated tube current modulation (CAREDose 4D) and automated tube voltage modulation (CAREKV) were enabled. Image acquisition was prospectively triggered to the patient's ECG at 30–80% of the R-R interval. Image series were reconstructed at 30–35% R-R and 70–80% R-R intervals [18] with a section thickness of 0.75 mm, a reconstruction increment of 0.5 mm, and a medium soft-tissue convolution reconstruction kernel (I26f). Patients received 60 mL of iopromide (Ultravist 370 mg I/mL, Bayer Schering Pharma) via injection into an antecubital vein using a 20-gauge catheter with a flow rate of 5 mL/s. Contrast administration was immediately followed by 40 mL of saline solution injected at 5 mL/s. The bolus tracking technique was employed by placing a region of interest in the aortic root in order to detect bolus arrival. Image acquisition began 4 s after an attenuation threshold of 100 Hounsfield Units was achieved.

Image analysis

Image quality assessment was performed in consensus by two observers with 17 (observer 1, L.J.Z.) and 2 (observer 2, F.Z.) years of experience using a four-point Likert scale (4 =

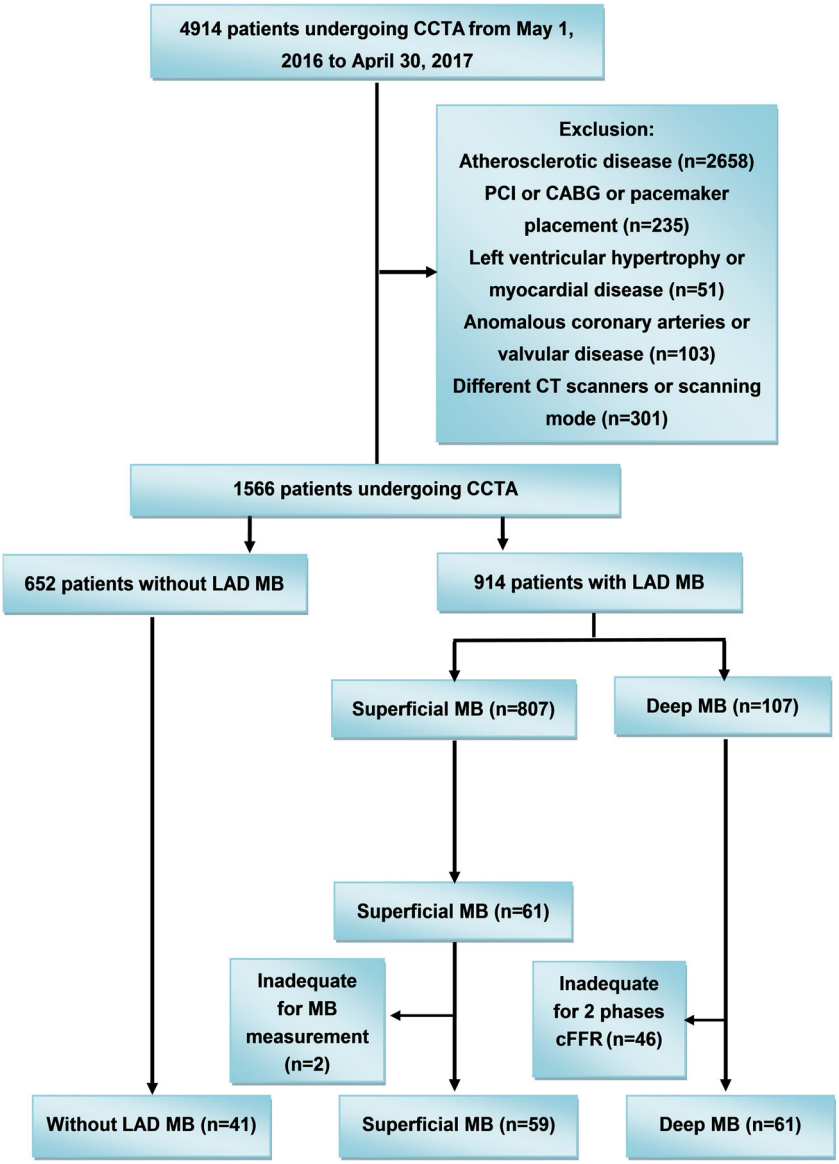

Fig. 1 Flow chart of the study. LAD, left anterior descending artery; MB, myocardial bridging; FFR, fractional flow reserve. Age- and sex- matched controls (without LAD MB) and superficial MB groups were selected according to deep MB group

excellent; 3 = good; 2 = acceptable; 1 = nondiagnostic) [19]. All MB measurements were performed on a dedicated workstation (Syngo Via, Siemens Healthcare). The location, depth, and length of MB were measured. MB location was defined as the distance from the LAD ostium to the MB entrance. The depth of MB was defined as the thickness at the deepest region from the surface of the covering myocardial tissue to the tunneled artery. MB length was defined as the distance of the tunneled artery from the entrance to the exit. These measurements were performed in axial images and curved planar reformats. MB was classified according to the depth of the tunneled segment beneath the epicardial surface, with ≤ 2 mm defined as superficial and > 2 mm defined as deep [1, 3, 12] (Fig. 1). When the overlying myocardium was thinner than or equal to 1 mm, a MB depth of 1 mm was recorded for further quantitative analysis. MB location and length were determined in the vertical long-axis plane (Fig. 1). In addition, MB muscle index was calculated as MB length (mm) × MB depth (mm) for superficial and deep MB [10]. MB stenosis was calculated as: [(coronary artery diameter proximal to MB - the minimal diameter of MB)/coronary artery diameter proximal to MB] × 100% [13]. To evaluate the degree of systolic compression, the systolic compression index was defined as [(minimal diastolic diameter - minimal systolic diameter)/diastolic diameter] [18].

cFFR modeling and measurements

cFFR calculations were performed on routine CCTA datasets using a software prototype (cFFR, version 3.0.0, Siemens Healthcare). The software is based on an artificial intelligence deep-machine-learning (DML) platform for the noninvasive computation of FFR values using existing CCTA data [20, 21]. Briefly, the algorithm had been trained using a

synthetically generated database of over 12,000 different coronary artery anatomies with randomly placed stenotic lesions among the different coronary branches and bifurcations. A reduced-order computational fluid dynamics (CFD) model was used to compute the pressure and flow distribution for each coronary tree. Subsequently, quantitative features of the coronary anatomy and computed FFR values were extracted at each location along the coronary tree, and the DML algorithm was trained to learn the relationship between the FFR values and quantitative anatomic features. Based on this training, FFR values for a new dataset can be predicted in a short period of time (2.4 ± 0.44 s) [22].

After CCTA datasets were successfully loaded, centerline and luminal contours for the entire coronary tree were automatically generated. The centerline and luminal contour are fundamental and critical information for the accurate computation of FFR values. Importantly, the observer can manually modify both if they were not initially optimized. The general diagnostic performance of the software has been tested in previous studies [23, 24]. cFFR values were determined by observer 2 (F.Z.), while centerline and luminal contours were verified by a second experienced observer 1 (L.J.Z.). Once all centerlines and contours were accepted, a color-coded coronary tree with corresponding FFR values was automatically generated. FFR measurements were obtained in segments 10 mm proximal to a MB, in MB segments with the most marked stenosis (if not stenosed, the mid-tunneled segment was selected), and in segments 10 mm distal to the MB (Fig. 1). Each cFFR measurement was performed three times and the average value was used for the final analysis. Abnormal values for cFFR were defined as ≤ 0.80 [15, 25–27]. Morphologic factors associated with abnormal cFFR values in the diastolic and systolic CCTA image series were analyzed.

Statistical analysis

Statistical analyses were performed using commercial software (Version 19.0; SPSS). The Kolmogorov-Smirnov test was conducted to assess the normality of quantitative data. Quantitative variables were expressed as mean ± SD if normally distributed, while median and inter-quartile range (M(QU-QL)) was provided for non-normally distributed data. Categorical variables were expressed as frequencies or percentages, with differences analyzed using Pearson's Chi-squared test or the likelihood ratio when appropriate. For normally distributed data, independent sample *t* tests, paired *t* tests, or ANOVA tests were used for the comparisons between two or three groups, if appropriate. The independent samples nonparametric test was used to analyze non-normally distributed data. For ANOVA tests, if the variance analysis revealed significant differences, post hoc analysis was performed for inter-group comparisons. Patient demographics and anatomical data were analyzed using binary logistic regression analysis and reported as odds ratios (OR) with their 95% confidence interval (CI). The forward stepwise selection was applied by using the likelihood ratio test with Akaike's information criterion as the stopping rule in multivariable analysis. Receiver operating characteristic (ROC) curve analysis was performed to analyze the role of statistically significant variables in detecting MB with normal or abnormal cFFR values using the method of DeLong et al [28]. A p value ≤ 0.05 was considered statistically significant.

Results

Patient demographics

A total of 120 patients (52.4 ± 11.0 years, 68% male) with LAD MB and 41 controls (53.4 ± 11.5 years, 54% male) were included. There were no significant differences between controls and MB subjects for age, sex, diabetes, hypertension, smoking, and hypercholesterolemia (all $p > 0.05$). Patient demographics are illustrated in Table 1.

Anatomical and cFFR features of MB

CCTA image quality was rated good or excellent in all 161 patients considering we had excluded studies unsuitable for cFFR analysis beforehand. Anatomical features of LAD MB are presented in Table 2. Deep MB was closer to the LAD ostium with more severe systolic and diastolic stenosis compared to superficial MB (all $p < 0.05$). MB length between the two groups was not different ($p = 0.20$).

Abnormal cFFR values were found in 29 patients (49.2%) in the superficial MB group and 40 patients (65.6%) in the deep MB group ($p = 0.069$). There were no abnormal cFFR values in the control group. cFFR values in deep MB segments were significantly different in systole and diastole ($p = 0.003$), while cFFR values for the other groups showed no differences between cardiac phases (all $p > 0.05$) (Table 2, Fig. 2). However, compared to controls, decreased cFFR values were observed in MB and distal segments in both MB groups in both cardiac phases. Notably, the pattern of reduced cFFR values was especially prominent in segments distal to the MB (Table 2, Fig. 2) (systole: MB segments: 0.97 (0.95–0.97), controls vs. 0.94 (0.90–0.96), superficial, $p = 0.001$; 0.97 (0.95–0.97), controls vs. 0.91 (0.83–0.95), deep, $p < 0.001$; distal segments: 0.92 (0.90–0.94), controls vs. 0.82 (0.71–0.89), superficial, $p < 0.001$; 0.92 (0.90–0.94), controls vs. 0.74 (0.60–0.89), deep, $p < 0.001$; diastole: MB segments: 0.96 (0.95–0.97), controls vs. 0.95 (0.91–0.96) superficial, $p = 0.002$, 0.96 (0.95–0.97), controls vs. 0.94 (0.91–0.96), deep, $p < 0.001$, distal segments: 0.93 (0.90–0.94), controls vs. 0.84 (0.69–0.92), superficial $p < 0.001$, 0.93 (0.90–0.94),

Table 1 Patient demographics

Parameters	Controls ($n = 41$)	MB ($n = 120$)		p value
		Superficial ($n = 59$)	Deep ($n = 61$)	
Age, years	53.4 ± 11.5	50.7 ± 11.9	54.0 ± 9.9	0.237
Sex (male), n (%)	22 (53.7)	37 (62.7)	44 (72.1)	0.158
Diabetes, n (%)	2 (4.9)	6 (10.2)	14 (23.0)	0.021*
Hypertension, n (%)	9 (22.0)	13 (22.0)	22 (36.1)	0.151
Smokers, n (%)	2 (4.9)	6 (10.2)	7 (11.5)	0.511
Hypercholesterolemia, n (%)	5 (12.2)	11 (18.6)	11 (26.2)	0.210

*An inter-group statistically significant difference was found between controls and deep MB ($p = 0.014$), while no significant differences were indicated for other inter-group comparisons ($p = 0.337$ and $p = 0.06$)

controls vs. 0.82 (0.68–0.90), deep, $p < 0.001$)). However, between the MB groups, no differences were observed for cFFR values in nearly all measured locations, aside from the MB segment ($p = 0.018$). Figure 3 provides three representative cases showing CCTA and cFFR features of the LAD both with and without MB.

Predictors of abnormal cFFR

Table 3 presents clinical and anatomical features of MB patients with and without abnormal cFFR values (≤ 0.80). Compared to MB patients with normal cFFR values, greater MB depth, length, and muscle index, as well as systolic were found in MB patients with abnormal cFFR values. There were no differences in clinical features, MB location, diastolic stenosis, or systolic compression index between groups (both $p > 0.05$). Results from the binary logistic regression analysis are illustrated in Fig. 4. MB length (OR = 1.06, 95% CI 1.03–1.11; $p = 0.001$) and systolic stenosis (OR = 1.04, 95% CI 1.01–1.07; $p = 0.021$) were the main predictors for abnormal cFFR.

We further analyzed MB systolic stenosis (model 1) and MB length (model 2) and the combination of them (model 3) for predicting abnormal cFFR using ROC analysis. The AUCs of each model were 0.647 (95% CI 0.549–0.744; $p = 0.050$), 0.726 (95% CI 0.636–0.817; $p < 0.001$), and 0.774 (95% CI 0.689–0.858; $p < 0.001$), respectively. Model 1 showed improved prediction of abnormal cFFR compared with MB

Table 2 Anatomical and cFFR features of myocardial bridging

Parameters	Controls ($n = 41$)	MB ($n = 120$)		p value
		Superficial ($n = 59$)	Deep ($n = 61$)	
Anatomical features				
MB depth, mm	–	1.0 (1.0–1.4)	2.9 (2.3–3.7)	< 0.001*
MB length, mm	–	30.3 (23.6–44.5)	34.8 (25.5–43.1)	0.200
MB muscle index	–	40.7 ± 20.7	118.3 ± 64.1	< 0.001*
MB location, mm	–	35.7 (30.1–45.6)	29.2 (25.4–35.6)	<0.001*
Systole MB stenosis, %	–	32.0 ± 11.6	42.5 ± 14.1	< 0.001*
Diastole MB stenosis, %		25.1 ± 10.4	32.5 ± 13.2	0.001*
Systolic compression index	–	0.1 (0.0–0.2)	0.2 (0.1–0.3)	0.029*
cFFR				
Systole				
Proximal to MB	0.99 (0.99–0.99)	0.99 (0.98–0.99)	0.99 (0.98–0.99)	0.173
MB	0.97 (0.95–0.97)	0.94 (0.90–0.96)	0.91 (0.83–0.95)	< 0.001*
Distal to MB	0.92 (0.90–0.94)	0.82 (0.71–0.89)	0.74 (0.60–0.89)	< 0.001*
Diastole				
Proximal to MB	0.99 (0.99–0.99)	0.99 (0.98–0.99)	0.99 (0.98–0.99)	0.011*
MB	0.96 (0.95–0.97)	0.95(0.91–0.96)	0.94 (0.91–0.96)	< 0.001*
Distal to MB	0.93 (0.90–0.94)	0.84 (0.69–0.92)	0.82 (0.68–0.90)	< 0.001*

Data are presented as mean ± SD or median with inter-quartile range

MB, myocardial bridging; *LAD*, left anterior descending artery; –, unavailable data

*Indicating significant difference

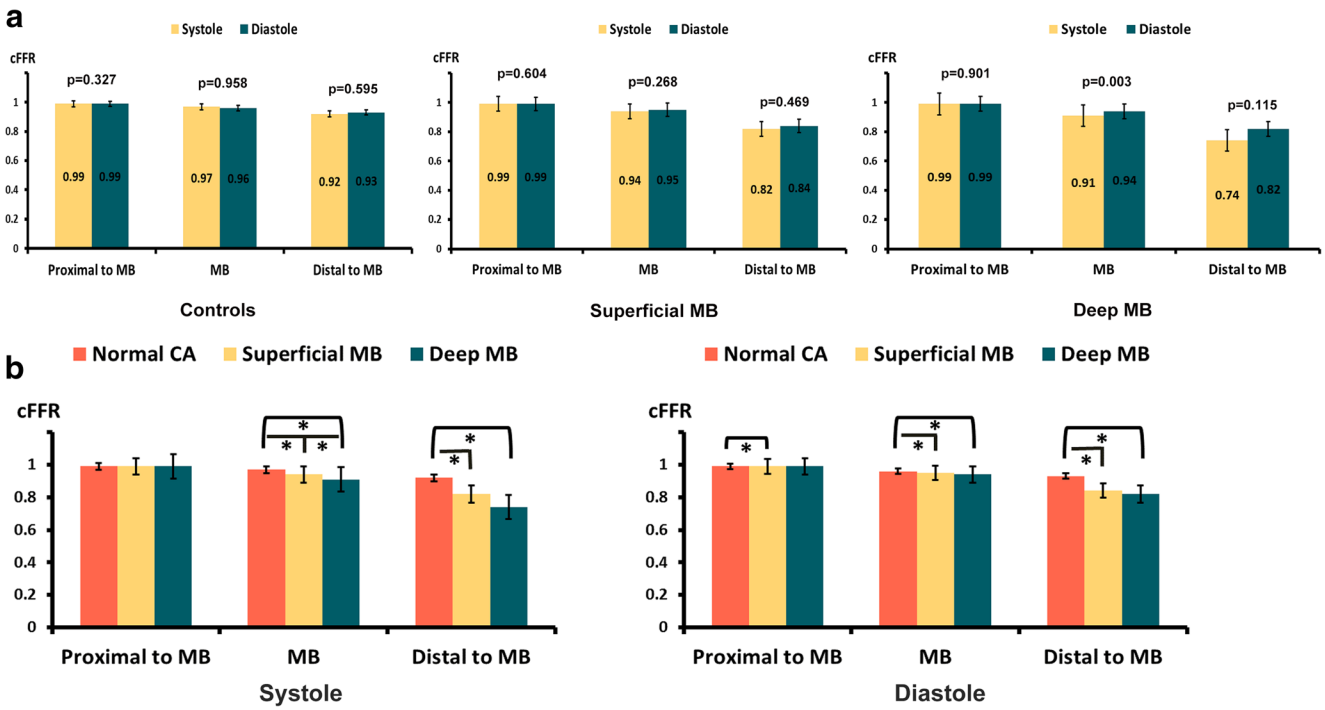

Fig. 2 Comparison of cFFR features. **a** For all cohorts, only cFFR values in deep MB segments demonstrated a significant difference between cardiac phases ($p = 0.003$). **b** Decreased cFFR values were observed in MB segments and segments distal to the MB in both cardiac phases among the three groups. CA, coronary artery; MB, myocardial bridging

systolic stenosis ($p = 0.0047$). There were no significant difference between the AUCs of model 1 and model 2 ($p = 0.2139$) or between model 2 and model 3 ($p = 0.1015$) (Fig. 5).

Clinical relevance

Table 3 depicts the various chest pain etiologies between MB patients with either normal or abnormal cFFR values. MB patients with abnormal cFFR values showed a higher prevalence of typical angina (18.8% vs 3.9%, $p = 0.023$) and were less frequently asymptomatic (27.5% vs. 47.1%, $p = 0.035$) compared to MB patients with normal cFFR values. Two MB patients with normal cFFR values developed syncope and one patient had palpitations. In MB patients with abnormal cFFR values, two patients had syncope and six patients developed palpitations.

Discussion

Our study found that both superficial and deep MBs can lead to abnormal cFFR values, especially in the segment distal to the MB. In addition, MB length and systolic stenosis were found to be the main contributors to abnormal cFFR values, the combination of them demonstrates moderate predictive performance. Importantly, MB patients with abnormal cFFR values had a higher prevalence of typical angina than patients with normal cFFR values, suggesting cFFR as a tool to gauge the clinical relevance of MB. Indeed, previous studies have elucidated the role of invasive FFR for assessing the severity and effects of MBs [1, 15, 29]. However, to the best of our knowledge, the use of cFFR in the setting of MB has not been previously studied [8].

Results from our investigation, mainly those regarding the decreased cFFR values in specific segments, are in line with previous results from studies using invasive FFR [1]. Specifically, previous investigations reported that both superficial and deep LAD MB can cause abnormal FFR values, especially in segments distal to the MB [1]. This indicates that the longer and deeper the MB, the more likely that it will be hemodynamically significant. We found a significant cFFR difference in cFFR values measured distally to the MB segment during systole between patients in the superficial and deep MB groups. This may be due to the reduction of the lumen diameter caused by myocardial contraction in systole, which can be seen as a

Fig. 3 CCTA and cFFR features of the left anterior descending coronary artery with and without myocardial bridging. **a** Normal left anterior descending coronary artery (LAD) in a 60-year-old woman showing normal course and cFFR values (0.88, 0.88) of the distal LAD in both cardiac phases. **b** Superficial MB in the mid-segment of the LAD in a 54-year-old woman. The MB depth is 0.7 mm and the MB length is 34.3 mm. Abnormal cFFR values (0.73, 0.77) are observed distal to the bridge in both systole and diastole, respectively. **c** Deep MB in the mid-segment of the LAD in an 81-year-old man. The MB depth is 3.1 mm and the MB length is 50.4 mm. Abnormal cFFR values (0.67, 0.66) distal to the MB are observed in both systole and diastole, respectively. CPR, curve planar reformation; scFFR, systolic cFFR; dcFFR, diastolic cFFR

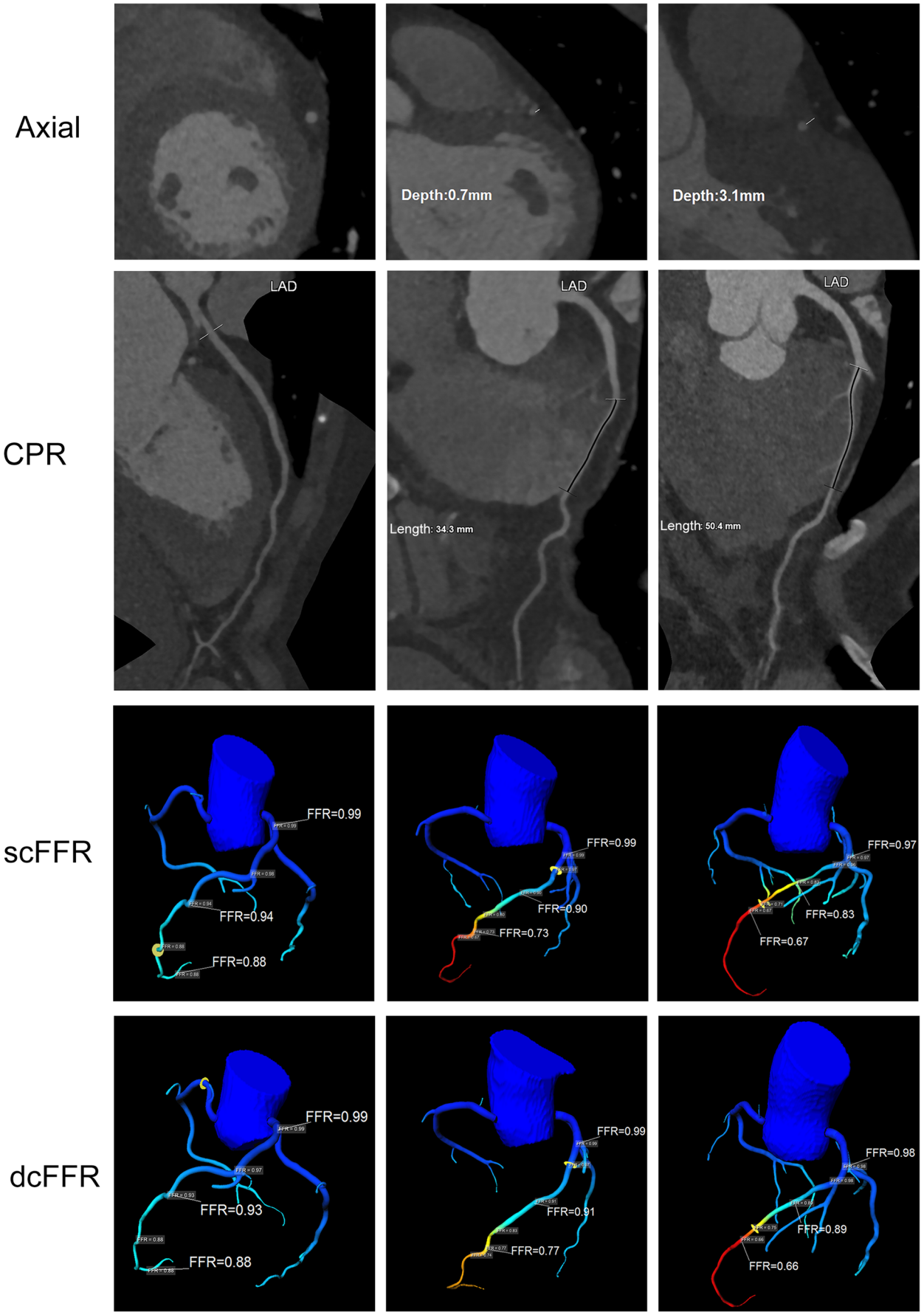
Axial
Depth:0.7mm
Depth:3.1mm
CPR
LAD
LAD
LAD
Length: 34.3 mm
Length: 50.4 mm
scFFR
FFR=0.99
FFR=0.94
FFR=0.88
FFR=0.99
FFR=0.90
FFR=0.73
FFR=0.97
FFR=0.83
FFR=0.67
dcFFR
FFR=0.99
FFR=0.93
FFR=0.88
FFR=0.99
FFR=0.91
FFR=0.77
FFR=0.98
FFR=0.89
FFR=0.66

Table 3 Clinical and anatomical features between myocardial bridging with and without abnormal cFFR values (≤ 0.80)

	MB with normal cFFR ($n = 51$)	MB with abnormal cFFR ($n = 69$)	p value
Baseline characteristics			
Age, years	50.8 ± 11.4.8	53.5 ± 10.6	0.187
Sex (male), *n* (%)	39 (76.5)	42 (60.9)	0.079
Diabetes, *n* (%)	8 (15.7)	12 (17.4)	> 0.999
Hypertension, *n* (%)	17 (33.3)	18 (26.1)	0.421
Smokers, *n* (%)	7 (13.7)	6 (8.7)	0.392
Hypercholesterolemia, *n* (%)	14 (27.5)	13 (18.8)	0.278
Chest pain			
Typical angina, *n* (%)	2 (3.9)	13 (18.8)	0.023*
Atypical angina, *n* (%)	9 (17.6)	9 (13.0)	0.606
Nonanginal chest pain, *n* (%)	13 (25.5)	20 (29.0)	0.836
No chest pain, *n* (%)	24 (47.1)	19 (27.5)	0.035*
Syncope, *n* (%)	2 (3.9)	2 (1.4)	
Palpitation, *n* (%)	1 (2.0)	6 (8.7)	
MB anatomical features			
MB depth, mm	1.7 (1.0–2.4)	2.2 (1.0–3.3)	0.044*
MB length, mm	29.1 ± 11.3	40.8 ± 16.8	< 0.001*
MB muscle index	46.1 (32.4–69.1)	80.9 (42.5–151.0)	< 0.001*
MB location, mm	33.3 (29.0–39.4)	31.4 (26.9–40.1)	0.583
Systole MB stenosis, %	32.9 ± 11.6	40.6 ± 14.6	0.003*
Diastole MB stenosis, %	26.6 ± 10.5	30.5 ± 13.5	0.085
Systolic compression index	0.12 (0.03–0.19)	0.13 (0.06–0.31)	0.060

MB, myocardial bridging; *LAD*, left anterior descending artery

*Indicating significant difference

"stenosis" and translated to "pressure" loss across the anatomical model by the computational modeling.

Notably, our study did not detect a relationship with other variables such as MB location, MB depth, MB muscle index, or arterial compression for causing abnormal cFFR values. Previous studies have found that patients with a long or deep MB did not necessarily demonstrate strong dynamic compression resulting in significant hemodynamic disturbances [12, 30]. In contrast, some patients with only a short or thin MB had a considerable degree of arterial compression, presumably depending on the variable function and anatomic direction of bridging muscle cells, as well as the three-dimensional geography of the tunneled artery and the surrounding cardiac structures [12, 30]. We speculate that the discrepancies between our current findings and others can be attributed to the patient inclusion criteria. Specifically, our study included LAD MB without any other abnormality, excluding patients with atherosclerotic plaque by CCTA, while other investigations included patients with nonobstructive CAD [5]. Additionally, noninvasive cFFR values were acquired during both cardiac phases, compared to the invasive FFR values collected solely in diastole with the use of dobutamine stress, potentially resulting in discrepancies.

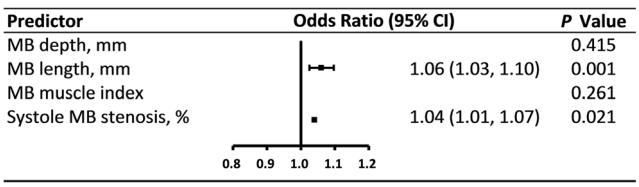

Fig. 4 Predictors for abnormal cFFR in patients with myocardial bridging. LAD, left anterior descending artery; MB, myocardial bridging; CI, confidence interval

Although our study was underpowered with regard to long-term follow-up outcomes to clarify the prognostic role of cFFR in MB patients, our observations have been suggested by a recent study by Agrawal et al In the pediatric study cohort, the authors reported that invasive FFR may help in risk stratification of patients with anomalous aortic origins of a coronary artery or MB [31]. Thus, it is plausible that cFFR holds potential as a tool to stratify MB patients, both with and without myocardial ischemia.

Our study has certain limitations. First, the retrospective nature and small sample size of the study limit the interpretation of the results. Second, the current study did not focus on the diagnostic accuracy of cFFR in a MB setting with invasive FFR or functional tests used as reference standard [32, 33]. Third, in this study, we applied a deep-machine-learning (DML)-based noninvasive cFFR tool in patients with MB. These results were not compared with other cFFR techniques such as computational fluid dynamics (CFD) modeling (HeartFlow, Inc.). However, a

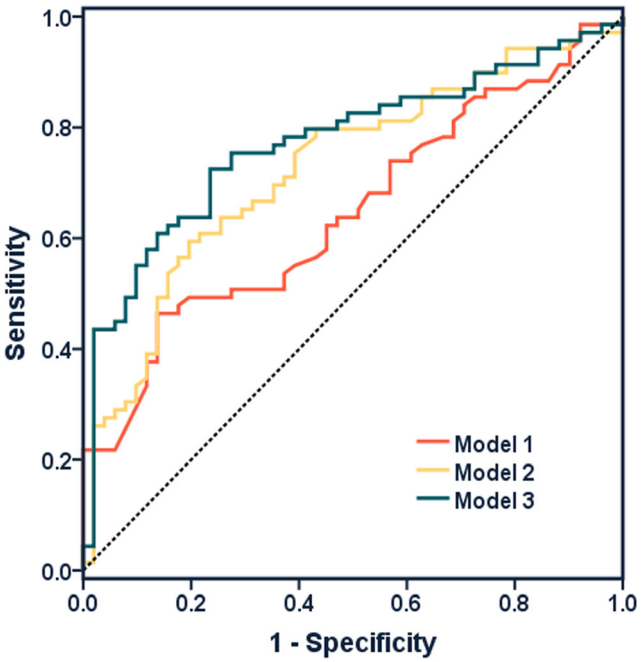

Fig. 5 ROC analysis of anatomical features of myocardial bridging in predicting abnormal cFFR. Model 1: MB systolic stenosis. Model 2: MB length. Model 3: MB systolic compression index + MB length. The AUCs of each model were 0.647 (95% CI 0.549–0.744; $p = 0.050$), 0.726 (95% CI 0.636–0.817; $p < 0.001$), and 0.774 (95% CI 0.689–0.858; $p < 0.001$), respectively. Model 3 shows improved prediction of abnormal cFFR compared with model 1 ($p = 0.005$). There was no significant difference between model 1 and model 2 ($p = 0.214$) or between model 2 and model 3 ($p = 0.102$)

recent study showed the DML-based FFR algorithm performed equally in detecting lesion-specific ischemia when compared with the CFD based FFR approach [23]. Fourth, our study did not clarify the relationship between atherosclerotic plaque and MB. Lastly, we were unable to determine long-term follow-up to investigate the prognostic value of cFFR measurements on the outcome of MB patients to guide management going forward.

In conclusion, we found that MB causes a higher prevalence of abnormal cFFR values and has an association with the clinical presentation of patients with MB. Thus, cFFR has the potential to enhance our understanding of MB and factors that render this condition of clinical relevance.

Funding This study has received funding by The National Key Research and Development Program of China (2017YFC0113400 for L.J.Z.).

Compliance with ethical standards

Guarantor The scientific guarantor of this publication is Long Jiang Zhang.

Conflict of interest UJS is a consultant for and/or receives research support from Astellas, Bayer, General Electric, Guerbet, HeartFlow, and Siemens Healthineers. The other authors have no conflicts of interest to disclose.

Statistics and biometry Meng Jie Lu has significant statistical expertise.

Informed consent Written informed consent was obtained from all subjects (patients) in this study.

Ethical approval Institutional Review Board approval was obtained.

Methodology
- retrospective
- observational
- performed at one institution

References

1. Forsdahl SH, Rogers IS, Schnittger I et al (2017) Myocardial bridges on coronary computed tomography angiography—correlation with intravascular ultrasound and fractional flow reserve. Circ J 81:1894–1900
2. Nakanishi R, Rajani R, Ishikawa Y, Ishii T, Berman DS (2012) Myocardial bridging on coronary CTA: an innocent bystander or a culprit in myocardial infarction? J Cardiovasc Comput Tomogr 6:3–13
3. Dimitriu-Leen AC, van Rosendael AR, Smit JM et al (2017) Long-term prognosis of patients with intramural course of coronary arteries assessed with CT angiography. JACC Cardiovasc Imaging 10:1451–1458
4. Rihal C, Ammash N (2017) Intramural course of coronary arteries: a bridge too far no more. JACC Cardiovasc Imaging 10:1459–1460
5. Rubinshtein R, Gaspar T, Lewis BS, Prasad A, Peled N, Halon DA (2013) Long-term prognosis and outcome in patients with a chest pain syndrome and myocardial bridging: a 64-slice coronary computed tomography angiography study. Eur Heart J Cardiovasc Imaging 14:579–585
6. Li Y, Yu M, Zhang J, Li M, Lu Z, Wei M (2017) Non-invasive imaging of myocardial bridge by coronary computed tomography angiography: the value of transluminal attenuation gradient to predict significant dynamic compression. Eur Radiol 27:1971–1979
7. Corban MT, Hung OY, Eshtehardi P et al (2014) Myocardial bridging: contemporary understanding of pathophysiology with implications for diagnostic and therapeutic strategies. J Am Coll Cardiol 63:2346–2355
8. Tarantini G, Migliore F, Cademartiri F, Fraccaro C, Iliceto S (2016) Left anterior descending artery myocardial bridging: a clinical approach. J Am Coll Cardiol 68:2887–2899
9. Wang Y, Lv B, Chen J et al (2013) Intramural coronary arterial course is associated with coronary arterial stenosis and prognosis of major cardiac events. Arterioscler Thromb Vasc Biol 33:439–444
10. Ishikawa Y, Akasaka Y, Suzuki K et al (2009) Anatomic properties of myocardial bridge predisposing to myocardial infarction. Circulation 120:376–383
11. Leschka S, Koepfli P, Husmann L et al (2008) Myocardial bridging: depiction rate and morphology at CT coronary angiography—comparison with conventional coronary angiography. Radiology 246:754–762
12. Kim PJ, Hur G, Kim SY et al (2009) Frequency of myocardial bridges and dynamic compression of epicardial coronary arteries: a comparison between computed tomography and invasive coronary angiography. Circulation 119:1408–1416
13. Konen E, Goitein O, Sternik L, Eshet Y, Shemesh J, Di Segni E (2007) The prevalence and anatomical patterns of intramuscular coronary arteries: a coronary computed tomography angiographic study. J Am Coll Cardiol 49:587–593
14. Gould KL, Johnson NP (2015) Myocardial bridges: lessons in clinical coronary pathophysiology. JACC Cardiovasc Imaging 8:705–709
15. Tarantini G, Barioli A, Nai Fovino L et al (2018) Unmasking myocardial bridge–related ischemia by intracoronary functional evaluation. Circ Cardiovasc Interv 11:e006247

16. Kurata A, Coenen A, Lubbers MM et al (2017) The effect of blood pressure on non-invasive fractional flow reserve derived from coronary computed tomography angiography. Eur Radiol 27:1416–1423
17. Lee HJ, Hong YJ, Kim HY et al (2012) Anomalous origin of the right coronary artery from the left coronary sinus with an interarterial course: subtypes and clinical importance. Radiology 262:101–108
18. Liu SH, Yang Q, Chen JH, Wang XM, Wang M, Liu C (2010) Myocardial bridging on dual-source computed tomography: degree of systolic compression of mural coronary artery correlating with length and depth of the myocardial bridge. Clin Imaging 34:83–88
19. Zhang LJ, Wang Y, Schoepf UJ et al (2016) Image quality, radiation dose, and diagnostic accuracy of prospectively ECG-triggered high-pitch coronary CT angiography at 70 kVp in a clinical setting: comparison with invasive coronary angiography. Eur Radiol 26:797–806
20. Duguay TM, Tesche C, Vliegenthart R et al (2017) Coronary computed tomographic angiography-derived fractional flow reserve based on machine learning for risk stratification of non-culprit coronary narrowings in patients with acute coronary syndrome. Am J Cardiol 120:1260–1266
21. Solecki M, Kruk M, Demkow M et al (2017) What is the optimal anatomic location for coronary artery pressure measurement at CT-derived FFR? J Cardiovasc Comput Tomogr 11:397–403
22. Itu L, Rapaka S, Passerini T et al (2016) A machine-learning approach for computation of fractional flow reserve from coronary computed tomography. J Appl Physiol (1985) 121:42–52
23. Tesche C, De Cecco CN, Baumann S et al (2018) Coronary CT angiography-derived fractional flow reserve: machine learning algorithm versus computational fluid dynamics modeling. Radiology 288:64–72
24. Kruk M, Wardziak Ł, Demkow M et al (2016) Workstation-based calculation of CTA-based FFR for intermediate stenosis. JACC Cardiovasc Imaging 9:690–699
25. Tonino PA, De Bruyne B, Pijls NH et al (2009) Fractional flow reserve versus angiography for guiding percutaneous coronary intervention. N Engl J Med 360:213–224
26. Collet C, Miyazaki Y, Ryan N et al (2018) Fractional flow reserve derived from computed tomographic angiography in patients with multivessel CAD. J Am Coll Cardiol 71:2756–2769
27. Tesche C, De Cecco CN, Albrecht MH et al (2017) Coronary CT angiography-derived fractional flow reserve. Radiology 285:17–33
28. DeLong ER, DeLong DM, Clarke-Pearson DL (1998) Comparing the areas under two or more correlated receiver operating characteristic curves: a nonparametric approach. Biometrics 44:837–845
29. Escaned J, Cortés J, Flores A et al (2003) Importance of diastolic fractional flow reserve and dobutamine challenge in physiologic assessment of myocardial bridging. J Am Coll Cardiol 42:226–233
30. Halliburton SS, Abbara S, Chen MY et al (2011) SCCT guidelines on radiation dose and dose optimization strategies in cardiovascular CT. J Cardiovasc Comput Tomogr 5:198–224
31. Agrawal H, Molossi S, Alam M et al (2017) Anomalous coronary arteries and myocardial bridges: risk stratification in children using novel cardiac catheterization techniques. Pediatr Cardiol 38:624–630
32. Takx RAP, Celeng C, Schoepf UJ (2018) CT myocardial perfusion imaging: ready for prime time? Eur Radiol 28:1253–1256
33. Dey D, Gaur S, Ovrehus KA et al (2018) Integrated prediction of lesion-specific ischaemia from quantitative coronary CT angiography using machine learning: a multicentre study. Eur Radiol 28: 2655–2664